Human Model-Based Active Driving System in Vehicular Dynamic Simulation

Hideyuki Kimpara, *Member, IEEE*, Kenechukwu C. Mbanisi, *Student Member, IEEE*, Jie Fu, *Member, IEEE*, Zhi Li, *Member, IEEE*, Danil Prokhorov, *Senior Member, IEEE*, and Michael A. Gennert, *Senior Member, IEEE*

***Abstract*— It is important that automotive engineers understand the interactions between active human maneuvering motions and vehicle dynamics, and how vehicle control affects the physical sensations of the human driver. This paper proposes a new system framework, the human model-based active driving system (HuMADS) for simulating human driver-vehicle interactions. HuMADS integrates the vehicle controller with models of vehicle dynamics and human biomechanics. It has an hierarchical closed-loop architecture for driver-vehicle control systems, including structures and contact interfaces of human and vehicle bodies. HuMADS is based on the OpenSim simulation platform. The developed system regulates the human model dynamics, such that the human model can react realistically to vehicle maneuver motions. The usability of the HuMADS is demonstrated through the simulation of coordinated gas/brake pedal operation and wheel-steering in highway driving tasks. The simulated vehicle dynamics and vehicle maneuvers are comparable with previously published experimental data of car-following driving. In addition, the proposed controllers successfully maintain the human body's balance inside the vehicle during vehicle maneuvers. We are convinced that the HuMADS has potential as a tool for the development of intelligent transportation systems and investigation of integrated safety.**

***Index Terms*— Human-vehicle systems, motion control, motion planning, systems modeling, vehicle dynamics.**

I. Introduction

DRIVER-ASSISTANCE or automated driving systems (ADS) have the potential to change the human-vehicle systems in driving tasks [1]–[4]. For example, intelligent driving systems may assist human drivers in vehicle maneuver actions to improve their safety and comfort, e.g., adaptive cruise control, automatic braking, lane departure warning, and lane-keeping assist [5]. In order to implement these complementary actions, these systems may need to actuate the vehicle controls causing the human driver to experience some mechanical forces or torque sensations from driving interfaces. Conversely, human drivers may need to regain control from the intelligent driving systems in order to maneuver in various driving situations. Therefore, vehicular driving behavior and resulting responses may be determined by interactive maneuvers from active actuation of both the human driver and intelligent driving systems [1]. Previous studies revealed human factors during transitions of driving authority from autonomous to manual driving modes may affect human's response times and driving performance [6]–[9]. However, conventional human-vehicle simulations mostly reflect the unidirectional interactions of vehicle dynamics on the human body, ignoring the effects of human dynamics on the vehicle. Therefore, a new bi-directional simulation framework for human-vehicle systems would be important for general transportation environments and developing intelligent driving systems.

This research focuses on rendering the whole-body coordination in vehicle maneuvers in response to the vehicle dynamics. For many driving tasks, a driver needs to coordinate the motion for gas and brake pedals with steering control, which results in complex motion responses ranging from passively maintaining body posture to actively maneuvering the vehicle according to traffic and road conditions. So far, there have been limited investigations of whole-body coordination that involves both passive and active motion reflex/control. Khatib *et al.* [10] studied whole-body coordination for complex balancing tasks [11], yet it is still unclear how to render active maneuver motion control in response to the dynamic environment. Previous research on mathematical modeling of the human driver has investigated motion coordination of the upper and lower extremities in driving tasks [12]–[15]. The lower extremities control vehicular longitudinal dynamics through coordination of leg and foot. The joint angles and torques of the hip, knee, and ankle control the angles and torques of the brake and gas pedals. Mulder *et al.* [12] studied the timing and control forces of vehicle pedal pressing motions and demonstrated that haptic gas pedal feedback improves driver vigilance in car-following tasks, which requires accurate real-time control of pedal position for maintaining inter-vehicle distance. To study human-vehicle interactions in simulation, it is important to equip the computational human model with low-level motion

Manuscript received September 12, 2018; revised January 9, 2019; accepted March 11, 2019. Date of publication April 11, 2019; date of current version May 1, 2020. This work was supported by the Collaborated Research Award from Toyota Motor North America R&D. The Associate Editor for this paper was C. Olaverri-Monreal. *(Corresponding author: Hideyuki Kimpara.)*

H. Kimpara was with Toyota Motor North America R&D, Ann Arbor, MI 48105 USA, and also with the Robotics Engineering Program, Worcester Polytechnic Institute, Worcester, MA 01609 USA. He is now with Toyota Central R&D Labs., Inc., Nagakute 480-1192, Japan (e-mail: hideyukikimpara@gmail.com).

K. C. Mbanisi, J. Fu, Z. Li, and M. A. Gennert are with the Robotics Engineering Program, Worcester Polytechnic Institute, Worcester, MA 01609 USA (e-mail: hkimpara@wpi.edu; kcmbanisi@wpi.edu; jfu2@wpi.edu; zli11@wpi.edu; michaelg@wpi.edu).

D. Prokhorov is with the Future Research Department, Toyota Motor North America R&D, Ann Arbor, MI 48105 USA (e-mail: danil.prokhorov@toyota.com).

This article has supplementary downloadable material available at http://ieeexplore.ieee.org, provided by the author.

Digital Object Identifier 10.1109/TITS.2019.2906294

planning and controllers that can render stable contacts and track desired human motion trajectories during vehicle maneuvers. In addition to motion planning and control, the framework for simulating human-vehicle interaction should also integrate a high-level decision-making module that accounts for the driver's cognitive behavior and performance according to theoretical driving models [14]–[17]. For instance, Salvucci proposed a hierarchical framework as a cognitive architecture that incorporates a driver model with components for vision-based vehicle control, environment monitoring, and vehicle maneuver decision-making [14]. However, since these studies usually represent human drivers as linear or non-linear time-delay functions, the desired maneuvers are guaranteed with the assumptions that no failures or errors in human behavior occur. On the other hand, motion measurement studies using human volunteer subjects reported accuracy and performance of pedal tasks depend on foot position and status at the beginning of maneuvers in real field driving environments [18]. In addition, further investigation using human volunteer subjects shows that human drivers' age, vehicle seat position, traffic signal phases, and driving sequences can alter the driver foot trajectory and time durations in either a laboratory testbed or out-of-laboratory with real running vehicles [19], [20]. Therefore, variability in human performance due to biomechanical or behavioral variability with disturbances in dynamics needs to be considered in human-vehicle systems [21].

In this paper, we propose a framework for an integrated human model-based active driving system (HuMADS) for rendering whole-body coordination in physical interaction between a human driver and a vehicle in typical driving scenarios. The main contributions of this paper are:

1) The design of a simulation framework for human driver-vehicle interactions that considers the effects of physical interactions due to inertial or contact forces and force equilibria on resulting maneuver performance and vehicle dynamics.
2) Implementation of robotics algorithms to connect theoretical driving models, biomechanical human models, and vehicle physics models.
3) Demonstration of human driver maneuvers and driving performance, and comparisons of simulated results with experimental data.

In order to achieve the aforementioned points, we employ a human body model platform and motion control algorithms based on robotics engineering enabling gas/brake pedals and steering maneuvers. Validating velocity and lateral positioning controls against previously published highway driving data [17], [22], we investigate driving performance, human motion control, actuated joint torques, and the resulting trajectories on the moving car. Other potential applications are for human-vehicle interfaces and applications for driver ergonomics and safety as well as for system information processing studies in vehicular dynamic simulations.

The structure of this article is as follows: Section II presents the model and system structure of HuMADS. Section III describes the vehicle test data and simulation condition parameters. Results and conclusions are presented in Sections IV and V, respectively.

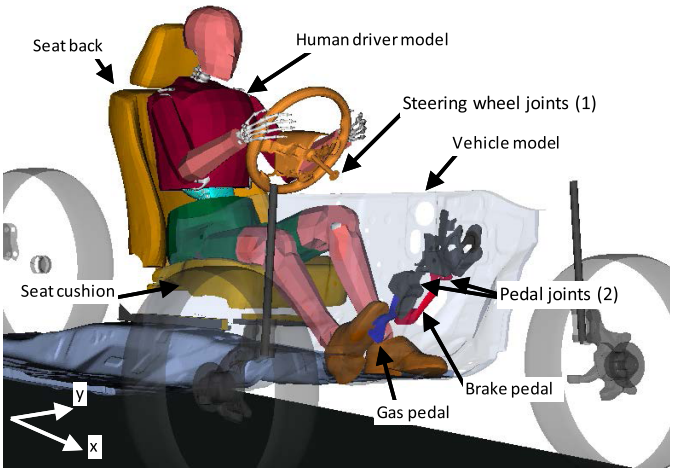

Fig. 1. Mechanical models of the human model-based active driving system (HuMADS) on OpenSim simulation platform.

II. Human-Vehicle Driving Framework of HuMADS

A. Simulation Platform

Various simulations of the human body have been proposed for automotive ergonomics or safety purposes. Chaffin and his group developed a digital human model for digital mock-up methods; however, their platforms were limited to static kinematic analyses [23]. The AnyBody simulation system was employed in biomechanical musculoskeletal analyses in the automotive research domain [24]. However, since that system was developed based on inverse dynamics theory, it is impossible to utilize it in a feedback control system. Finite element (FE) simulation and human body modeling were also used for automotive safety studies in [25]. Although FE human body models are good at soft contact and flexible body properties as well as forward dynamics simulations, they are inferior in computational speed. In addition, FE models generally require a remeshing process for any repositioning or reposturing of the human body. On the other hand, multibody models allow one to easily change model positions using state variables. In particular, OpenSim has capabilities of forward dynamics (FD) analysis as well as inverse kinematics (IK) and inverse dynamics (ID) analyses [26]–[28]. The Application Programming Interfaces (APIs) defined in OpenSim and SimBody allow programs to access parameters of the models and dynamics to calculate the equation of motions at runtime. Therefore, this study selected OpenSim as the simulation platform for the human-vehicle driving simulation system.

Because the targeted tasks of the driving system follow typical driving scenarios, the HuMADS in this study is assumed to represent an average-size human driving a regular passenger car in the highway traffic. Fig. 1 shows the mechanical models of the HuMADS in OpenSim, consisting of a human body with height of 1.8 m and weight of 77.4 kg, and 2012 Toyota Camry. The human body model has 31 degrees of freedom (DOF). These DOF are distributed among the neck (6 DOF), lumbar (3 DOF), upper extremities (4 DOF/each) and lower extremities (7 DOF/each). Muscle elements of OpenSim

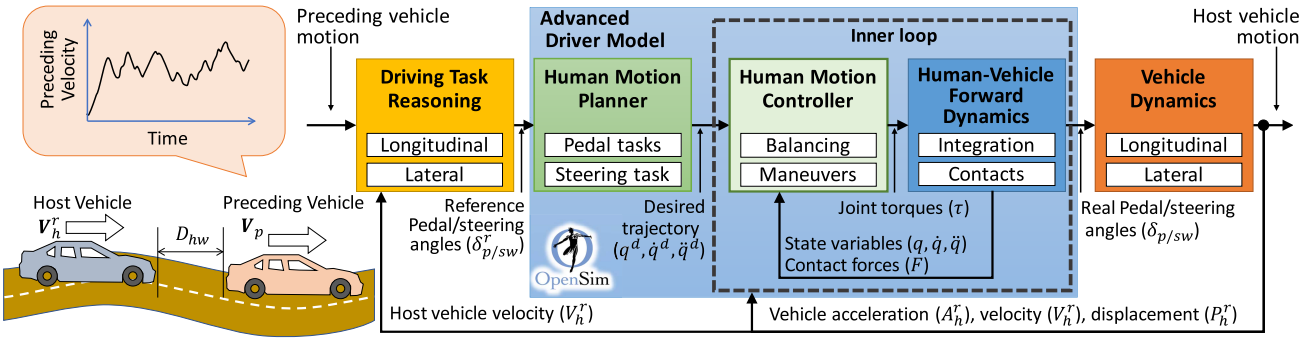

Fig. 2. Driver-vehicle control framework illustrated in the vehicle following drive task. Inputs are preceding vehicle velocity and pathway, and outputs are host vehicle velocity, lateral position and yaw angle.

human body models are replaced with ideal torque actuators at the joints for simplicity. The vehicle model, with three coordinate joints of pedals and steering wheel, is linked to the ground with three degrees of freedom of longitudinal (x) and lateral (y) translations and yaw rotation. Vehicle geometry and inertial properties come from a FE model of a Toyota Camry [29], [30]. This model includes major components of the vehicle exterior and interior, such as driver seat, pedals, and steering wheel. The joint center, mass center, and inertial properties for all components are estimated from material properties of the FE models. The joint stiffness characteristics of the gas and brake pedals are computed according to a non-linear viscoelastic with friction torque model. Pedal force characteristics against the displacement for gas and brake pedals agree with literature data [31], [32].

Our simulation defines the contact interfaces between the human body parts and vehicular interior instruments and components, including the gas and brake pedals. In particular, the contact geometries of the human body come from skin mesh models of the Hybrid III 50th percentile male dummy [33]. The contact forces are computed using the ElasticFoundationForce model [27], while the contact parameters are determined according to the data of the pendulum foot impact in [34]. Given the above setup, our simulation generates impact reaction forces consistent with the test results of a dummy foot with two loading speeds. Although the literature data compares dynamic responses of human bare feet and dummy bare feet, we assumed that the dummy bare feet data may be reasonable for general drivers' feet wearing shoes. The half-space contact geometry defined by OpenSim is used to represent soft contact interfaces on the seat cushion and back [35]. The human pelvis is mounted on the seat cushion using a weld joint, which constrains all degrees of freedom. Because this study employs driving on a highway as the primary task scenario, we assume that the human driver holds the steering wheel with both hands. Therefore, point-to-point force models are used to constrain the hands on the steering wheel with rotational freedom.

The aforementioned contact and constraint forces are defined by virtual bodies for the human body regions. Since the point contact forces are not clearly expressed by the current OpenSim, external force vectors F_{ext} are calculated by the 6-DOF joint reaction force outputs on the weld joint between the inertial and zero-mass virtual bodies.

B. Hierarchical Controller Structure and implementation

This study designed a high-fidelity model for the human driver's motions in normal driving scenarios as a vehicle-following task model with two vehicles as in Fig. 2. The preceding vehicle moves at velocity V_p, then the host vehicle follows the preceding vehicle with velocity V_h and headway distance D_{hw}. The interactions between human and vehicle models are built upon two controllers: the ***vehicle controller*** controls the longitudinal and lateral motions of the vehicle (i.e., accelerating, braking, lane following, etc.), while the ***advanced driver model*** based on the OpenSim platform controls the dynamic human driving motions accordingly. The vehicle controller is designed based on a linear feedback system with the **driving task reasoning** and **vehicle dynamics** models proposed by Saigo [17]. The human motion controller consists of a **human motion planner**, **human motion controller**, and **human-vehicle forward dynamics** analysis.

The outer loop layers, including the driving task reasoning, human motion planner, and vehicle dynamics are coded in Matlab, whereas the inner loop of human motion controller and human-vehicle forward dynamics are expressed in C++. In principle, one could have coded everything in one software environment, but we had already implemented our previous work [36] in Matlab. We decided to combine this paper's development in OpenSim and C++ with that of Matlab to prepare for future developments in multi-language environments. In order to achieve the multi-loop system with different models implemented in both C++ and Matlab, we synchronized them over sufficiently short sampling of 50Hz with adaptive-time-step Runge-Kutta-Merson integrator. We plan to make our software available in an on-line repository in the future.

C. Driving Task Reasoning

The Driving Task Reasoning layer, which is part of the ***vehicle controller***, computes the reference pedal δ^r_{pd} and steering angles δ^r_{sw} for longitudinal and lateral motion control individually.

For longitudinal motion, the host vehicle sets its reference velocity V^r_h to follow the preceding vehicle that moves at

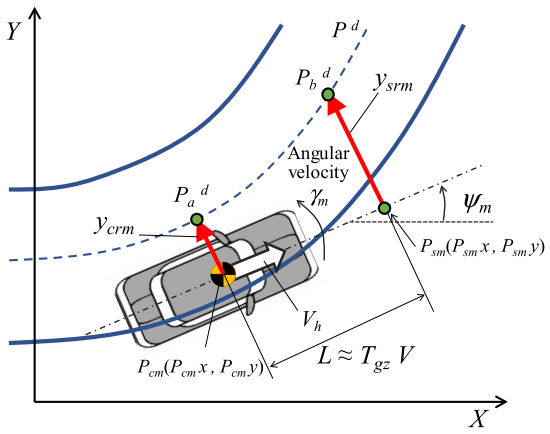

Fig. 3. Vehicle position and objective pathway.

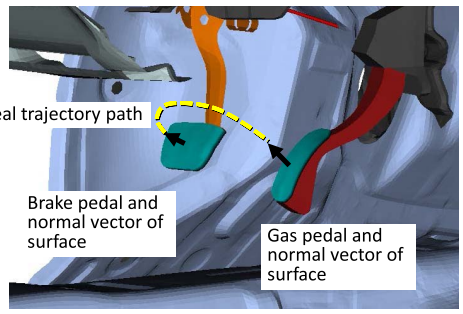

Fig. 4. Brake and gas pedal locations and ideal trajectory.

velocity V_p. D_{hw} and D^d_{hw} are the actual and desired headway distances between the preceding vehicle and host vehicle. The desired headway distance, D^d_{hw}, is determined based on the assumption that human drivers try to maintain a constant separation *in time* between their vehicle and the preceding one. This time separation is T^d_{hw}, typically 1.5 sec. The driver sets the desired headway distance D^d_{hw} based on own vehicle velocity V_h and time separation T^d_{hw}. The actual headway distance is related to the vehicle velocities as follows:

$$\dot{D_{hw}} = V_p - V_h. \tag{1}$$

The reference pedal angles δ^r_{pd} can be described by the following control equation:

$$\delta^r_{pd} + T_{pd}\dot{\delta}^r_{pd} = H_D\left\{D_{hw} - D^d_{hw}\right\} + H_V\left\{V_p - V^r_h\right\}, \tag{2}$$

where T_{pd} is time delay for human driver in pedal task, H_D and H_V are the gain constants for headway distance and vehicle velocity, respectively.

The lateral motion controller is a forward-gaze model on the highway (Fig. 3) based on the theory of vehicle dynamics described by Abe [37], which determines the yaw angle ψ_m and yaw rate (angular velocity) $\gamma_m\left(=\dot{\psi_m}\right)$ of the vehicle around the vertical axis to follow the objective pathway P^d in an X-Y coordinate system. The X-Y axes show the fixed plane coordinate on the ground, whereas x-y are local coordinate on the vehicle. The x and y axes represent longitudinal and lateral vehicle directions, respectively. The origin of the local frame is at the vehicular center of gravity (CG), P_{cm}. The lateral deflection of the vehicle current position P_{cm} from the objective pathway in the vehicle coordinate system is expressed as y_{crm} (Fig. 3). In addition, the expected vehicle position P_{sm} expressed in terms of the forward-gaze time duration T_{gz} as:

$$P_{sm} = P_{cm} + T_{gz} V R\left(\psi_m\right), \tag{3}$$

where the function $R\left(\psi_m\right)$ represents a rotational transformation of angle ψ_m. The lateral deflection of the expected position P_{sm} from the objective pathway in the vehicle coordinate system is expressed as y_{srm} (Fig. 3). Then the driver is assumed to set steering angle δ^r_{sw} proportional to the lateral deflections y_{srm} and y_{crm}.

$$\delta^r_{sw}(t) + T_{sw}\dot{\delta}^r_{sw}(t) = h_s y_{srm} + h_c y_{crm}, \tag{4}$$

where T_{sw} is time delay for human driver in steering task,h_s and h_c are gains for the driver corrective steering angle.

The reference pedal angles δ^r_p and steering angle δ^r_{sw} are achieved by the inner-loop motion planner and controller, described in the following subsection.

D. Human Motion Planner

The Human Motion Planner computes the desired joint angles q^d, angular velocities $\dot{q}^d$, and angular accelerations $\ddot{q}^d$ given the reference pedal angles δ^r_{pd} and steering angle δ^r_{sw} that control the longitudinal and lateral motions of a vehicle. To obtain those joint space variables, we first plan feasible 3D Cartesian trajectories of the hands and feet. Then we utilize inverse kinematics (IK) to determine the desired joint angles from the planned trajectories.

First, we plan feasible trajectories for the coordinated lower extremity joints that implement the motion for pedal pressing. In regular passenger vehicles, no obstacles exist around the driver's feet workspace other than the gas and brake pedals. However, the driver's right foot must approach pedal surfaces in consideration of each pedal's movable directions. Wu et al. reported that the foot-to-pedal trajectory describes a rounded curve that approaches the pedals from normal directions to the pedal surfaces [19]. Therefore, we assume that a typical task space trajectory of the foot during pedal switching is a continuous curve that connects the initial and end pose of the foot as shown in Fig. 4. The motion planner needs to convert the desired trajectory to a sequence of desired joint angles and angular velocities. Shown in Fig. 5, our motion planner uses 3D potential and force fields to generate the desired task space trajectory, which will be further converted to a joint space trajectory through inverse kinematics (IK).

We define a force field $F(p)$ as the sum of an attractive force F_{att} centered at the goal and a set of repulsive forces $F_{\text{rep},j}$ centered at regions of space to avoid, such as behind the pedals:

$$F(p) = F_{\text{att}}(p) + \sum\nolimits_j F_{\text{rep},j}(p). \tag{5}$$

In Fig. 5(a), we denote the current target position and center of attractor as p and C_{att}, respectively. The relative position of these points is denoted as $\overrightarrow{pC}_{\text{att}}$. Thus, the attractive force

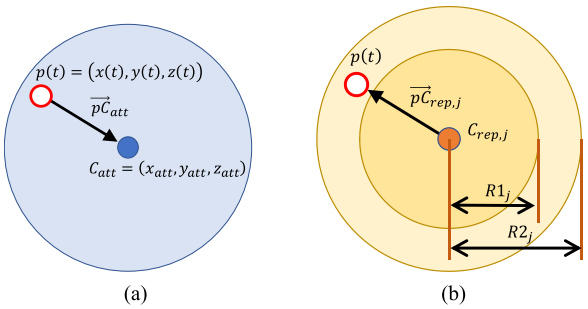

Fig. 5. Arrangements of current point with attractor and repulsions. (a) Current point p around attractive potential field. (b) Current point p around j^{th} repulsive potential field.

$F_{\text{att}}(p)$ can be computed as:

$$F_{\text{att}}(p) = \zeta \frac{\overrightarrow{pC}_{\text{att}}}{\left|\overrightarrow{pC}_{\text{att}}\right|}, \tag{6}$$

where ζ is a coefficient that indicates the strength of the attractive force, which always points in the goal direction.

In Fig. 5(b), the current target position and the j^{th} center of repulsion are denoted by p and $C_{\text{rep},j}$, respectively. The relative positions of these points are denoted as $\overrightarrow{pC}_{\text{rep},j}$. Thus, the j^{th} repulsive force $F_{\text{rep},j}(p)$ can be computed as:

$$F_{\text{rep},j}(p) = -\eta_j \frac{\overrightarrow{pC}_{\text{rep},j}}{\left|\overrightarrow{pC}_{\text{rep},j}\right|}. \tag{7}$$

where η_j is a term that indicates the strength of the repulsive force, which always points away from the center of repulsion. Term η_j comprises two components. One decreases linearly from 0 to distance $R2_j$; the other follows an inverse square law from 0 to distance $R1_j$. Combining these components based on the distance from each center of repulsion $\left|\overrightarrow{pC}_{\text{rep},j}\right|$ gives:

$$\begin{cases} \eta_j = \lambda_1 \dfrac{R1_j^2}{\left|\overrightarrow{pC}_{\text{rep},j}\right|^2} + \lambda_2 \dfrac{\left(R2_j - \left|\overrightarrow{pC}_{\text{rep},j}\right|\right)}{R2_j - R1_j} & : \left|\overrightarrow{pC}_{\text{rep},j}\right| < R1_j \\ \eta_j = \lambda_2 \dfrac{\left(R2_j - \left|\overrightarrow{pC}_{\text{rep},j}\right|\right)}{R2_j - R1_j} & : R1_j \le \left|\overrightarrow{pC}_{\text{rep},j}\right| < R2_j \\ \eta_j = 0 & : R2_j \le \left|\overrightarrow{pC}_{\text{rep},j}\right|. \end{cases} \tag{8}$$

Since the human driver is assumed to hold the steering wheel with both hands during driving on a highway, the hand positions are determined from transferred positions on the steering wheel. Therefore, desired hand positions are planned by required reference steering angle δ^r_{sw} during the driving.

In the regular highway driving task, the human driver can be assumed to maintain their initial posture, therefore the desired position and orientations of the head and torso bodies will also maintain their initial posture.

As the latter part of the motion planner, we employed OpenSim's IK analysis to obtain desired joint angles from planned trajectories. The OpenSim's IK analysis computes the joint angles q^d using the weighted least squares method, in order to fit the desired marker positions. Fig. 6 shows the virtual markers for positioning a human body with indicated weights. Since the pelvis is a base for the hierarchical human body model, three virtual markers of Hip and Belt positions for right and left have greater weights. We consider the top tip position (i.e., the Toe and Hand_1 in Fig. 6) as the end effector position of the lower and upper extremities and compute the desired trajectories. Ferber *et al.* [38] reported that the peak velocity of the ankle joint was 291 [degrees/s] in dorsiflexion. Since the distance between toe and ankle joint is 0.18 [m] in this model, this creates a foot velocity around 0.9 [m/s]. Therefore, discrete desired points of tip end p_t^d at time t are determined with intervals of time step and foot velocity. Given the desired discrete positions of the top tip, we further compute the desired discrete joint angles q^d through the inverse kinematics (IK) analysis. To calculate desired joint angular velocities $\dot{q}^d$ and angular accelerations $\ddot{q}^d$, we compute the polynomial curve function fitting with discrete joint angles and obtained differential variables. The other virtual markers such as Hand_2/3, Elbow, Heel, Tibia, Femur_bottom, Head top, and Gaze_R/L are placed in initial positions to keep the human body driving positioning.

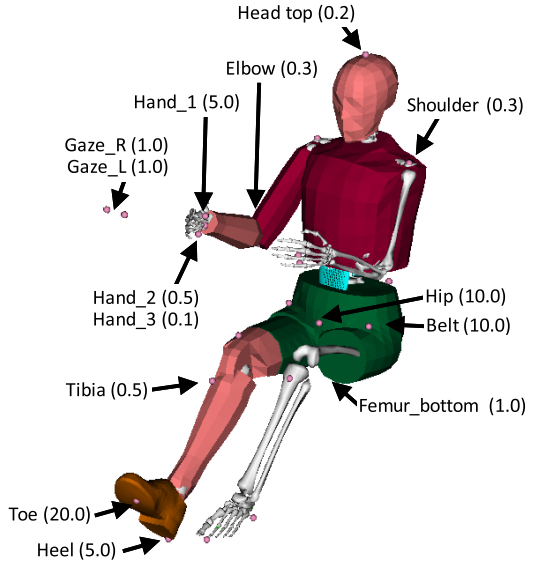

Fig. 6. Virtual markers for inverse kinematics (IK) analysis of human driving motions.

E. Human Motion Controller

The human motion controller layer computes the desired joint torques τ given the desired joint angles q^d, angular velocities $\dot{q}^d$, and angular accelerations $\ddot{q}^d$ of the vehicle maneuver motion. Through inverse dynamics, we compute the desired joint torque for the whole-body human driver model to maintain its body posture while tracking the desired trajectory for pedal pressing or switching. Inverse dynamics is one method of feedback linearization [39]. The inverse dynamics requires the mass, Coriolis forces, and gravity of a dynamic system. Specifically, the dynamics of an n-link rigid robot can be expressed as:

$$M(q)\ddot{q} + C(q, \dot{q}) + N(q) + J^T F_{ext} = \tau. \tag{9}$$

where q is the state variables in joint space, $M(q)$ is the mass matrix, $C(q, \dot{q})$ is the velocity vector which is the product of the Coriolis and Centrifugal force matrix and the velocity $\dot{q}$ of the state variables, $N(q)$ is the vector of torques due to gravity, J^T represents the system Jacobian matrix, F_{ext} captures the external forces, and τ is the joint torques.

Theidea of inverse dynamics introduced by Spong *et al.* [39] is to express τ as the function $f(q, \dot{q}, t)$. Therefore, the dynamics equation (9) can be modified by substituting $\ddot{q}$ for a new input a_q as follows:

$$\tau = M(q)\, a_q + C(q, \dot{q}) + N(q) + J^T F_{ext}. \tag{10}$$

Given the desired joint positions, velocities, and accelerations, our motion controller guarantees that:

$$\ddot{\tilde{q}} + K_D \dot{\tilde{q}} + K_P \tilde{q} + K_F J^T \tilde{F}_{ext} = 0, \tag{11}$$

where q^d is the vector of desired state variables, $\tilde{q}$ represents the error of state variables ($\tilde{q} = q - q^d$, $\dot{\tilde{q}} = \dot{q} - \dot{q}^d$, $\ddot{\tilde{q}} = \ddot{q} - \ddot{q}^d$), $\tilde{F}_{ext}$ is the error of the external forces ($\tilde{F}_{ext} = F_{ext} - F^{\mathrm{d}}_{ext}$), K_P, K_D and K_F are diagonal matrices of position, velocity, and force gains, respectively. To control a linear second-order system, we need to regulate a_q:

$$a_q = \ddot{q}^d - K_P\left(q - q^d\right) - K_D\left(\dot{q} - \dot{q}^d\right) - K_F J^T\left(F_{ext} - F^d_{ext}\right). \tag{12}$$

We assume that the human driver determines pedal positions based on force feedback and remembers – and therefore compensates for – the expected reaction forces from the pedals based on the pedal positions. Therefore, we designed the desired pedal force as a non-linear function of pedal positions $F_P\left(\delta^r_{pd}\right)$. In addition, the human driver may adjust the pedal position at the request of pedal position δ_{pd} from the driving task reasoning layer, therefore, the desired force is expressed as follows:

$$F^d_{ext} = F_P\left(\delta^r_{pd}\right) - K_{GP}\left(\delta_{pd} - \delta^r_{pd}\right), \tag{13}$$

where the function F_P represents a function of pedal angle and contact force relationship and K_{GP} is a pedal position gain. Due to complex contact phenomenon around the pedals, it was almost impossible to make the two force vectors exactly equal. We see from (12) that if the force gain K_F is too small, the desired feedforward force prediction F^d_{ext} does not contribute much to the pedal motion; if K_F is too large, the kinematics become unstable. Alternatively, we assigned greater value for gain K_{GP} to emphasize the desired force directions. Similarly, to adjust the actual steering wheel angle at the request of steering wheel angle δ_{sw}, the desired force is expressed as follows:

$$F^d_{ext(steer)} = -K_{GSW}\left(\delta_{sw} - \delta^r_{sw}\right), \tag{14}$$

where K_{GSW} is a steering wheel angle gain.

The vehicle motions given from the vehicle dynamics in Fig. 2 are produced by the coordinated actuation forces F_h in the longitudinal, lateral, and yaw directions. The required actuation forces are calculated as follows:

$$F_h = M_h\left\{A^r_h - K_{hP}\left(P_h - P^r_h\right) - K_{hD}\left(V_h - V^r_h\right)\right\}. \tag{15}$$

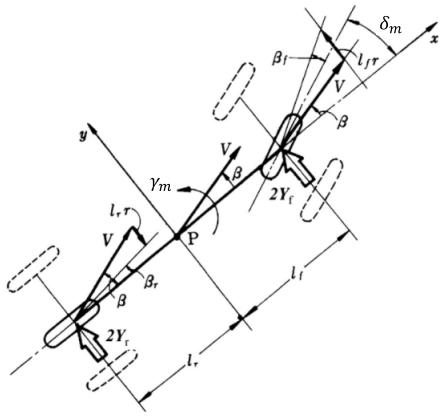

Fig. 7. Equivalent bicycle model for vehicular lateral motion.

where M_h is the inertia matrix of the vehicle body, A^r_h, V^r_h, and P^r_h are the reference variables of vehicle acceleration, velocity, and displacement from the vehicle dynamics layer, and K_{hP} and K_{hD} are position and velocity gains, respectively.

F. Vehicle Dynamics

The human-vehicle forward dynamics layer uses the whole-body human model to simulate the human driver's forward kinematics and dynamics in order to predict the actual control angles of the pedal δ_p. Next, the vehicle dynamics layer, which is another part of the vehicle controller, converts the driver's commanded pedal angles δ_p and steering wheel angle δ_{sw} to vehicle dynamics. The host vehicular acceleration A^r_h can be expressed as follows:

$$A^r_h + T_g \dot{A^r_h} = K_g \delta_p, \tag{16}$$

where K_g and T_g are the gain and time constants of the pedal function, respectively. When air resistance C_{air} is considered, the host vehicle velocity V^r_h can be expressed as:

$$C_{air} V^r_h + \dot{V^r_h} = A^r_h. \tag{17}$$

Vehicular lateral motions are expressed based on the equivalent bicycle model in Fig. 7. The actual front tire angle δ_m is determined by the actual steering wheel angle δ_{sw} and gear ratio n:

$$\delta_m = \delta_{sw}/n. \tag{18}$$

The angle β between velocity vector V and longitudinal direction x in Fig. 7 is called the side slip angle. Considering the component of acceleration in the lateral direction, the lateral dynamics are expressed as:

$$mV\left(\dot{\beta} + \gamma_m\right) = 2F_f + 2F_r, \tag{19}$$

where m is vehicle mass, F_f and F_r are the lateral forces on front and rear tires, and γ_m is the yaw rate.

The lateral forces also result in a moment in the yaw direction around the vehicle CG, given by:

$$I\dot{\gamma}_m = 2l_f F_f - 2l_r F_r, \tag{20}$$

where I is moment of inertia, l_f and l_r are distances from vehicle CG to front and rear wheel axes, respectively.

The lateral forces F_f and F_r on each tire are proportional to the side slip angles on the front β_f and rear β_f tires; the proportionality constants are denoted as the cornering stiffness K_f and K_r. Since rotational directions of all angles are expressed as positive in the anticlockwise direction in the vehicle coordinate system (Fig. 7), side slip angles and lateral forces can be expressed as positive and negative, respectively. Therefore, the lateral forces are described as:

$$\begin{aligned} F_f &= -K_f\beta_f = -K_f\left(\beta + l_f\gamma_m/V - \delta_m\right) \\ F_r &= -K_r\beta_r = -K_r\left(\beta - l_r\gamma_m/V\right). \end{aligned} \tag{21}$$

Then the equations of dynamics in (19) and (20) can be expanded by a Laplace transformation, where $\beta(s)$, $\gamma(s)$, and $\delta(s)$ are the Laplace transforms for β, γ_m, and δ_m:

$$\begin{aligned} &\left\{mVs + 2\left(K_f + K_r\right)\right\}\beta(s) \\ &\quad + \left\{mV + \frac{2}{V}\left(l_fK_f - l_rK_r\right)\right\}\gamma(s) = 2K_f\delta(s) \\ &2\left(l_fK_f - l_rK_r\right)\beta(s) + \left\{Is + \frac{2\left(l_f^2K_f + l_r^2K_r\right)}{V}\right\}\gamma(s) \\ &\quad = 2l_fK_f\delta(s) \end{aligned} \tag{22}$$

The side slip angle transfer function $G_\beta(s)$ is:

$$\begin{aligned} G_\beta(s) &= \frac{\beta(s)}{\delta(s)} = G_\beta(0)\frac{1+T_\beta s}{1+\frac{2\zeta s}{\omega_n}+\frac{s^2}{\omega_n^2}}, \\ G_\beta(0) &= \frac{1+\frac{m}{2l}\frac{l_f}{l_rK_r}V^2}{1+KV^2}\frac{l_r}{l}, T_\beta = \frac{IV}{2ll_rK_r}\frac{1}{1-\frac{m}{2l}\frac{l_f}{l_rK_r}V^2} \end{aligned} \tag{23}$$

where ω_n and ζ are expressed as follows:

$$\begin{aligned} \omega_n &= \frac{2l}{V}\sqrt{\frac{K_fK_r\left(1+KV^2\right)}{mI}}, \\ \zeta &= \frac{m\left(l_f^2K_f + l_r^2K_r\right) + I\left(K_f + K_r\right)}{2l\sqrt{mIK_fK_r\left(1+KV^2\right)}}, \\ K &= -\frac{m}{2l^2}\frac{l_fK_f - l_rK_r}{K_fK_r}, \quad l = l_f + l_r. \end{aligned} \tag{24}$$

The yaw rate transfer function $G_\gamma(s)$ is:

$$\begin{aligned} G_\gamma(s) &= \frac{\gamma(s)}{\delta(s)} = G_\gamma(0)\frac{1+T_\gamma s}{1+\frac{2\zeta s}{\omega_n}+\frac{s^2}{\omega_n^2}}, \\ G_\gamma(0) &= \frac{1}{1+KV^2}\frac{V}{l}, \quad T_\gamma = \frac{ml_fV}{2lK_r}. \end{aligned} \tag{25}$$

When the current vehicle position is described as $P_{cm}(t)$, the vehicle velocity $\dot{P}_{cm}(t)$ in ground coordinates can be described with vehicle speed V and yaw angle $\psi_m(t)$ and side slip angle $\beta(t)$ as follows:

$$\begin{aligned} \dot{P}_{cm,x}(t) &= V\cos\left(\beta(t) + \psi_m(t)\right), \\ \dot{P}_{cm,y}(t) &= V\sin\left(\beta(t) + \psi_m(t)\right). \end{aligned} \tag{26}$$

The resulting vehicle motions dynamics are fed back to the driving task reasoning layer and inner loop of human motion planner and human-vehicle forward dynamics.

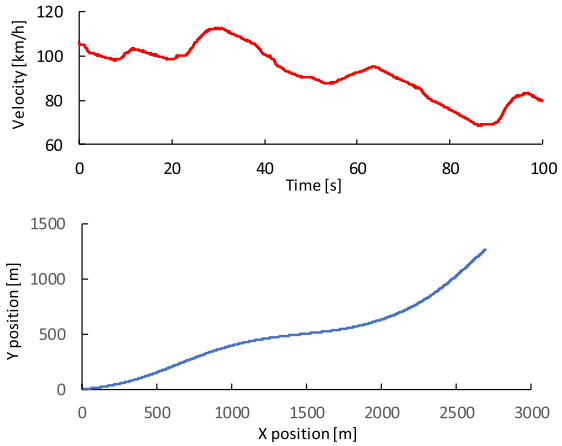

Fig. 8. Input variables of preceding vehicle velocity and driving pathway.

TABLE I
PARAMETERS FOR THE DRIVING TASK REASONING LAYER

Parameter	Symbol	Values
Time separation [s]	T_{hw}^d	1.4
Gain for distance difference [%/m]	H_D	2.0
Gain for velocity difference [%/(m/s)]	H_V	6.0
Time delay for human driver in pedal task [s]	T_{pd}	0.4
Steering compensation gain [rad/m]	h_s, h_c	0.1
Forward-gaze time duration for steering task [s]	T_{gz}	1.4
Time delay for human driver in steering task [s]	T_{sw}	0.1

III. SIMULATION SETUP

In [17], Saigo validated the driver-vehicle model based on a linear feedback system against the experimental data obtained from human subjects driving on expressways. Our study follows that simulation setup for vehicle dynamics and therefore compares the simulation result to the dataset used in the previous study (Fig. 8). Saigo [17], Saigo *et al.* [22] obtained vehicle dynamics and driver operation data such as host vehicle longitudinal and lateral accelerations, vehicle velocity, yaw rate, headway distance, gas pedal position, brake pedal pressure, and steering angle directly from the controller area network (CAN), which is a robust data bus in the vehicle. The preceding vehicle velocity was calculated from adding host vehicle velocity to the differential headway distance value. The road pathway was obtained from front facing camera images.

Tables I and II show the parameters used for the driver-vehicle model. In our simulation, the brake pedal gain K_b is set the same as the gas pedal gain K_g in order to compare vehicle performance with that reported in [17]. One significant difference in parameters between [17] and this simulation concerns the time constants for the human driver in the pedal and steering tasks. In [17] these were set to$T_{pd} = 1.0$ and $T_{sw} = 0.4$, respectively, to account for the time delay in force transmission. However, that model did not include human body dynamics, which our model explicitly includes. Our more realistic model effectively introduces time delays in the human body dynamics; thus, we assume smaller delay time constants in TABLE I. The pedal position gain K_{GP} for equation (13) is

TABLE II
PARAMETERS FOR THE VEHICLE DYNAMICS LAYER

Parameter	Symbol	Values
Time constant for gas pedal function [s]	T_g	0.008
Gain of gas and brake pedal function [(m/s)/%]	K_g, K_b	0.028
Air resistance [s^{-1}]	C_{air}	0.11
Wheel base [m]	l	2.85
Distance from vehicle C.G. to front tire [m]	l_f	1.33
Distance from vehicle C.G. to rear tire [m]	l_r	1.52
Vehicle mass [kg]	M	1690
Steering gear ratio [-]	n	15.7
Cornering force on front tire [N/rad]	C_f	44145
Cornering force on rear tire [N/rad]	C_r	61999
Moment of inertia [kg m^2]	I	72.7

determined as 3000 and 2000 N/rad for brake and gas pedals, respectively.

An instance of an OpenSim class to manage the execution of a simulation is declared with the Runge-Kutta-Merson integrator through the SimBody API. We choose a range of integration time steps from 0.5 [μs] to 0.5 [ms].

The update frequency for reference variables between the outer and inner loops is 50 Hz, while the human motion controller inner loop updates the desired (reference) joint variables and contact forces at 1 kHz.

Our simulation renders the motion of the human driver upper and lower extremities on a simulated moving car. In order to represent driving a real car on the road, the OpenSim vehicle model is also actuated with reference vehicle kinematic data using Equation (15).

IV. RESULTS AND DISCUSSION

A. Overall Kinematics and Dynamics

The results of applying the Student t-test between the vehicle kinematics of the OpenSim model and reference variables from the vehicle dynamics layer yield correlation coefficients of almost 1.0, with p values less than 0.01. These matches between physical vehicle model and vehicle dynamics layer is favorable for human-vehicle interaction studies.

Fig. 9 shows simulated driver motions and driving maneuvers. The motion planner and motion controller successfully generated a typical trajectory for the foot tip to travel between the gas and brake pedals while turning the steering wheel and balancing the whole human body.

B. Resulting Vehicle Maneuvers and Performances

Fig. 10 compares human driving maneuvers and resulting vehicle kinematics in terms of pedal position, vehicle velocity, steering angle, and vehicle lateral displacement error against desired pathway among current simulation models and previous model of Saigo [17] and human subject (driver# R3) data from an experimental test [17]. This driving scenario contains decelerating from 110 km/h to 70 km/h within a 60 s time segment. Driving task reasoning may contain several functions of sensing, cognition, and high-level task planning. This study employed a linear model for providing reference variables of pedal positions and steering angle, as was done

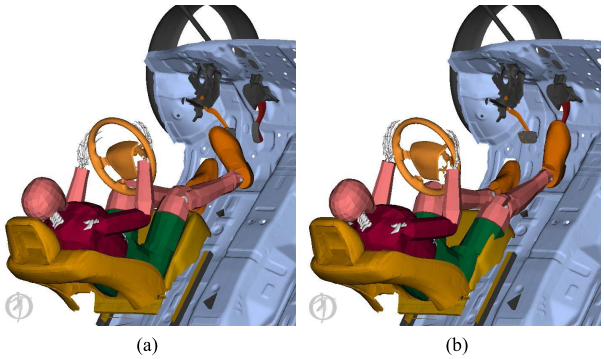

Fig. 9. Human body model posture while driving a vehicle model. (a) Pressing brake pedal with 10 deg turning steering wheel to the left. (b) Pressing gas pedal with 5.6 deg turning steering wheel to the right.

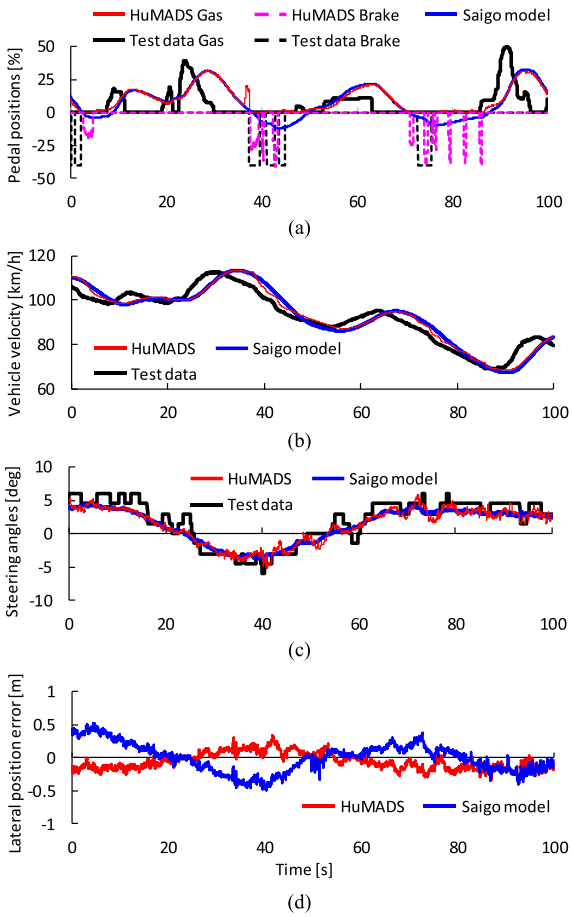

Fig. 10. Comparison of driving performance and resulting vehicle performance among the HuMADS model on the moving car, the previous model from Saigo [17], and experimental data. (a) Gas and brake pedal positions [%]. (b) Host vehicle velocity [km/h]. (c) Steering angle [deg]. (d) Lateral vehicle position error against desired pathway [m].

in the previous study [17]. Therefore, pedal position changes during continuous gas pedal operation are comparable between the current HuMADS model and Saigo's model.

Although brake pedal position of the test data indicates only record of braking switch in Fig. 10(a), brake pedal operations are observed around 1, 40, and 75 [s] from the experimental data. Simulation results from HuMADS expressed brake pedal performances with peaks of striking pedals at the similar

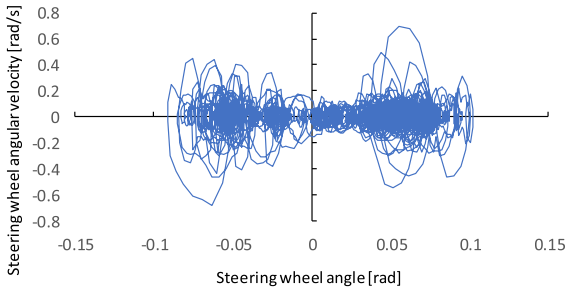

Fig. 11. Phase trajectory plot of steering wheel motion.

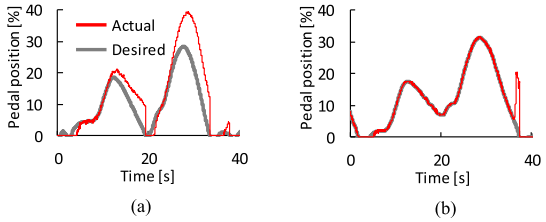

Fig. 12. Comparisons of real gas pedal position and desired pedal position between without and with force feedback. (a) Without force feedback. (b) With force feedback.

timings as the test data. There exists a time delay when switching the foot position to another pedal, which is caused by the motion planner and parameters of the motion control layer. In contrast, the previous model exhibited smoother pedal position changes because there is no foot transfer from gas pedal to brake pedal.

Overall steering angle curves expressed by simulation models run along the line of test data (Fig. 10c). As can be seen from a phase trajectory plot of steering wheel motions in Fig. 11, the steering wheel motions are qualitatively stable. The vehicle driving performance of vehicle lateral positions simulated by the HuMADS were comparable with that obtained from the previous model. The peak errors were 0.35 m and 0.53 m observed from HuMADS and Saigo models, respectively.

The current implementation of HuMADS employs a linear feedback controller and a rigid physical vehicle model in a highway-driving scenario to elucidate the human driver-vehicle interactions. Since the bicycle model is non-holonomic as equation (26), Model Predictive Control (MPC) is typically used for driving task reasoning [13], [40]. However, because the steering angle δ^r_{sw} will be small, as shown in Fig. 10c, i.e. less than 0.1 radian, changes of slip angle $\beta(t)$ and yaw angle $\psi_m(t)$ will also be small. With sufficiently fast sampling, 50 Hz in our case, we may reasonably assume a piece-wise linearization, which allows us to apply a linear controller to this bicycle model for the current driving task.

On the other hand, since all system functions are designed individually in an outer loop, it is possible to exchange a part of HuMADS for other advanced models. For example, Yi et al. expressed aggressive driving maneuvers with a driving scenario of sharp turning curves [41]. Their vehicle model could express full rotational motions considering tire contact and slip models using the CarSim simulator. Future studies with the HuMADS may be able to address the human driver-vehicle interactions with other driving maneuvers and scenarios.

C. Force Feedback Control in Driving Task

Fig. 12 shows comparisons of real pedal position and desired pedal position between cases without and with force feedback controls. Pedal position gain K_{GP} plays an important role in maintaining desired pedal positions. When a smaller position gain K_{GP} is used, the gas and brake pedal positions cannot reach the desired values. Since human drivers have high haptic sensitivity on the hands and feet [42], we believe that force feedback control and gain variables around steering wheel and pedals are essential to perform driving maneuvers properly.

D. Motion Plan and Time Delay of Human Driver

The time constants for time delay models of human driver in driving task reasoning layer are assumed to be 0.4 s and 0.1 s for the pedal and steering tasks, respectively. Macadam summarized human time delays as 0.18 s and 0.3-0.4 s of the visual and auditory response times under near ideal condition, respectively [43]. However, Scott [44], [45] reported that response time delays due to sensory feedback such as passive joint movements or skin contacts are generally quicker than those requiring visual feedback based on neuroscience experiments . Since this proposed model can divide cognition processes from vision and force feedback into driving task reasoning and internal force feedback of human body control, the time constants from [17] may be dispersed among the feedback sources with appropriate factors. Each function of driving task reasoning, motion planner, and motion controller are clearly separated, so that time delays of each individual function are also clearly specified in HuMADS. Further validation studies may provide better understanding about the effects of biological time delays on driving performance and interaction with vehicle dynamics.

On the other hand, the preceding velocity curves used for this study were almost comparable with host vehicle velocity curves because the preceding vehicle velocity was estimated as a summation of host vehicle velocity and difference values of headway distance changes. Therefore, the vehicle velocity calculated by the models are always delayed with respect to test results.

In addition, further motion analysis from learning algorithms and the design of high-level motion planners are necessary for reproducing more human-like driver behaviors. Even with the force feedback controller as currently implemented, the generated motions are still smoother than real human motions. A human motion study of vehicle pedal maneuvers revealed that complex foot motions can be decomposed into motion primitives and that it is possible to reproduce complex motions from learned motion libraries [36].

E. Vehicle Dynamics and Biomechanics of the Human Driver

This section introduces an example estimation of the relationships between vehicle motions and human driver's actuation efforts. Fig. 13 shows simulation results of vehicle

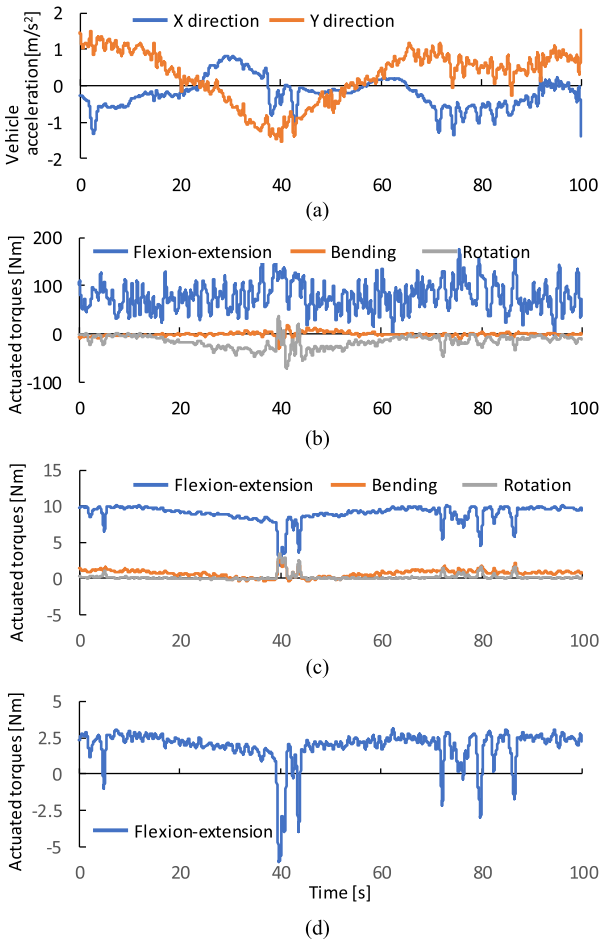

Fig. 13. Simulation results of vehicle acceleration and actuated joint torques on the lumbar, shoulder, and elbow joints. (a) Vehicle acceleration. (b) Actuated joint torques on the lumbar joint. (c) Actuated joint torques on the shoulder joint. (d) Actuated joint torque on the elbow joint.

acceleration on X and Y direction and actuated torques on the lumbar, shoulder, and elbow joints of a human driver body. The voluntary maximum joint torques of human subjects in a normal driving posture are believed to be around 80 Nm and 50 Nm for shoulder and elbow joints, respectively [46]. The expected actuated torques in HuMADS are around 10 Nm and 2.5 Nm, respectively (Fig. 13b,c), which are well within acceptable limits. The longitudinal acceleration (Fig. 13a) had significant deceleration pulses in accordance with the brake pedal maneuvers (Fig. 10a). The effects of these deceleration pulses were observed in flexion-extension joint torques on the shoulder and elbow joints. On the contrary, actuated joint torques on the lumbar joint did not express significant changes at the 1, 40, and 75 s marks. This result may agree with findings from an experimental study that hand constraints with the steering wheel can significantly reduce forward traveling distances of the driver upper body on strongly decelerated vehicles [47].

In general, human motions can be expressed as outputs from a closed-loop motor control system of humans with vision and sensory prediction feedbacks. Physiological sensors such as joint receptors, muscle spindle organs, Golgi tendon, and Renshaw cells may have analogs in robotics sensory systems of joint angle, velocity, actuator effort, and reaction forces [48], [49]. Because OpenSim includes biomechanical analysis feature such as adaptive scaling methods for individual subjects and musculoskeletal analysis, it may be possible to use biomechanical variables such as electromyogram (EMG) measurement for better understanding of human-vehicle dynamics.

V. Conclusions

This paper proposed a new framework of the Human model-based active driving system (HuMADS) for human driver-vehicle interactions including driving task reasoning, human driver motion, and resulting vehicle dynamics. We described how to connect theoretical driving vehicle models with biomechanical human and vehicle models based on force equilibria and dynamics. In the highway driving scenario, the HuMADS generated driving maneuvers and vehicle performance comparable to those of human subject test data. While the HuMADS behaves similarly to the real world driving data, further refinements of our framework are needed to improve overall fidelity to human-like motions. We are convinced that the HuMADS has potential as a future tool for development of intelligent transportation systems and investigation of integrated safety, and we hope to make it accessible to a wide audience of researchers in the future.

Acknowledgment

We appreciate Prof. Pongsathorn Raksincharoensak of Tokyo University of Agriculture and Technology permission to use the car-following experimental data collected by Dr. Saigo for this project. We thank Dr. Shintaro Saigo for his informative data. We also would like to thank team members of the National Center for Simulation in Rehabilitation Research (NCSRR) about their technical supports for OpenSim.

References

[1] I. Hideo, R. Pongsathorn, and I. Shintaro, "Intelligent driving system for safer automobiles," *J. Inf. Process.*, vol. 25, pp. 32–43, Jan. 2017
[2] S. B. McLaughlin, J. M. Hankey, and T. A. Dingus, "A method for evaluating collision avoidance systems using naturalistic driving data," *Accident Anal. Prevention*, vol. 40, no. 1, pp. 8–16, 2008.
[3] N. Kalra and S. M. Paddock, "Driving to safety: How many miles of driving would it take to demonstrate autonomous vehicle reliability?" *Transp. Res. A, Policy Pract.*, vol. 94, pp. 182–193, Dec. 2016.
[4] A. Best, S. Narang, L. Pasqualin, D. Barber, and D. Manocha. (2017). "AutonoVi: Autonomous vehicle planning with dynamic maneuvers and traffic constraints," [Online]. Available: https://arxiv.org/abs/1703.08561
[5] A. H. Eichelberger and A. T. McCartt, "Toyota drivers' experiences with dynamic radar cruise control, pre-collision system, and lane-keeping assist," *J. Saf. Res.*, vol. 56, pp. 67–73, Feb. 2016.
[6] T. Saito, T. Wada, and K. Sonoda, "Control authority transfer method for automated-to-manual driving via a shared authority mode," *IEEE Trans. Intell. Veh.*, vol. 3, no. 2, pp. 198–207, Jun. 2018.
[7] X. Yan, Y. Zhang, and L. Ma, "The influence of in-vehicle speech warning timing on drivers' collision avoidance performance at signalized intersections," *Transp. Res. C, Emerg. Technol.*, vol. 51, pp. 231–242, Feb. 2015.
[8] K. Zeeb, A. Buchner, and M. Schrauf, "What determines the take-over time? An integrated model approach of driver take-over after automated driving," *Accident Anal. Prevention*, vol. 78, pp. 212–221, May 2015.
[9] M. Blanco *et al.*, "Human factors evaluation of level 2 and level 3 automated driving concepts," Nat. Highway Traffic Safety Admin., Washington, DC, USA, Tech. Rep. DOT HS 812, 2015.

[10] O. Khatib, L. Sentis, J. Park, and J. Warren, "Whole-body dynamic behavior and control of human-like robots," *Int. J. Humanoid Robot.*, vol. 1, no. 1, pp. 29–43, 2004.
[11] M. Mansouri Boroujeni, "Dynamic simulation and neuromuscular control of movement: Applications for predictive simulations of balance recovery," Ph.D. dissertation, Univ. Tennessee, Knoxville, TN, USA, 2015.
[12] M. Mulder, D. A. Abbink, M. M. van Paassen, and M. Mulder, "Design of a haptic gas pedal for active car-following support," *IEEE Trans. Intell. Transp. Syst.*, vol. 12, no. 1, pp. 268–279, Mar. 2011.
[13] N. Mehrabi, R. S. Razavian, and J. McPhee, "Steering disturbance rejection using a physics-based neuromusculoskeletal driver model," *Vehicle Syst. Dyn.*, vol. 53, no. 10, pp. 1393–1415, 2015.
[14] D. D. Salvucci, "Modeling driver behavior in a cognitive architecture," *Hum. Factors*, vol. 48, no. 2, pp. 362–380, 2006.
[15] A. J. Pick and D. J. Cole, "A mathematical model of driver steering control including neuromuscular dynamics," *J. Dyn. Syst., Meas., Control*, vol. 130, no. 3, 2008, Art. no. 031004.
[16] B. Shi, L. Xu, and W. Meng, "Applying a WNN-HMM based driver model in human driver simulation: Method and test," *IEEE Trans. Intell. Transp. Syst.*, vol. 19, no. 11, pp. 3431–3438, Nov. 2018.
[17] S. Saigo, "Study on driving state estimation method with on-board driver behavior model," Ph.D. dissertation, Dept. Mech. Syst. Eng., Tokyo Univ. Agricult. Technol., Fuchu, Japan, 2014.
[18] C. Tran, A. Doshi, and M. M. Trivedi, "Modeling and prediction of driver behavior by foot gesture analysis," *Comput. Vis. Image Understand.*, vol. 116, no. 3, pp. 435–445, 2012.
[19] Y. Wu, L. N. Boyle, D. McGehee, C. A. Roe, K. Ebe, and J. Foley, "Modeling types of pedal applications using a driving simulator," *Hum. Factors*, vol. 57, no. 7, pp. 1276–1288, 2015.
[20] Y. Wu, L. N. Boyle, D. McGehee, C. A. Roe, K. Roe, and J. Foley, "Foot placement during error and pedal applications in naturalistic driving," *Accident Anal. Prevention*, vol. 99, pp. 102–109, Feb. 2017.
[21] T. A. Ranney, "Models of driving behavior: A review of their evolution," *Accident Anal. Prevention*, vol. 26, no. 6, pp. 733–750, 1994.
[22] S. Saigo, P. Raksincharoensak, and M. Nagai, "Investigation of inattentive driving estimation method by using longitudinal and lateral driver operational models," *SAE Int. J. Passenger Cars-Electron. Elect. Syst.*, vol. 6, no. 1, pp. 27–33, 2013.
[23] D. B. Chaffin, "Improving digital human modelling for proactive ergonomics in design," *Ergonomics*, vol. 48, no. 5, pp. 478–491, 2005.
[24] M. Damsgaard, J. Rasmussen, S. T. Christensen, E. Surma, and M. De Zee, "Analysis of musculoskeletal systems in the anybody modeling system," *Simul. Model. Pract. Theory*, vol. 14, no. 8, pp. 1100–1111, 2006.
[25] K. Yamada, M. Gotoh, Y. Kitagawa, and T. Yasuki, "Simulation of occupant posture change during autonomous emergency braking and occupant kinematics in frontal collision," in *Proc. Int. Res. Council Conf. Biomech. Injury*, 2016, pp. 261–274.
[26] S. L. Delp *et al.*, "OpenSim: Open-source software to create and analyze dynamic simulations of movement," *IEEE Trans. Biomed. Eng.*, vol. 54, no. 11, pp. 1940–1950, Nov. 2007.
[27] A. Seth *et al.*, "OpenSim: Simulating musculoskeletal dynamics and neuromuscular control to study human and animal movement," *Plos Comput. Biol.,* vol. 14, no. 7, 2018, Art. no. 1006223.
[28] M. A. Sherman, A. Seth, and S. L. Delp, "Simbody: Multibody dynamics for biomedical research," *Procedia Iutam*, vol. 2, pp. 241–261, Aug. 2011.
[29] R. Reichert, P. Mohan, D. Marzougui, C. D. Kan, and D. Brown, "Validation of a toyota camry finite element model for multiple impact configurations," SAE Tech. Paper 2016-01-1534, 2016.
[30] Center for Collision Safety and Analysis. (2016). *2012 Toyota Camry Detailed Finite Element Model*. George Mason University. [Online]. Available: https://www.ccsa.gmu.edu/models/2012-toyota-camry/
[31] H. P. Ho, "The influence of braking system component design parameters on pedal force and displacement characteristics," Ph.D. dissertation, School Eng., Des. Technol., Univ. Bradford, Bradford, U.K., 2016.
[32] *Heusinkveld Engineering. Product Catalog*. Accessed: Jan. 12, 2018. [Online]. Available: http://heusinkveld.com/
[33] LSTC. *Detailed FE Model of Hybrid III 50th Male Dummy LSTC. H3_50TH_DETAILED.151214_BETA_IntermediateRelease*. Accessed: Feb. 3, 2018. [Online]. Available: http://www.lstc.com/download
[34] P. Manning, A. Wallace, C. Owen, A. Roberts, C. Oakley, and R. Lowne, "Dynamic response and injury mechanism in the human foot and ankle and an analysis of dummy biofidelity," in *Proc. 16th Int. Tech. Conf. Enhanced Saf. Vehicles*, 1998, pp. 1960–1998.
[35] M. M. Verver, R. De Lange, J. F. A. M. van Hoof, and J. S. H. M. Wismans, "Aspects of seat modelling for seating comfort analysis," *Appl. Ergonom.*, vol. 36, no. 1, pp. 33–42, 2005.
[36] K. C. Mbanisi, H. Kimpara, T. Meier, M. Gennert, and Z. Li, "Learning coordinated vehicle maneuver motion primitives from human demonstration," in *Proc. IEEE/RSJ Int. Conf. Intell. Robots Syst. (IROS)*, Oct. 2018, pp. 6560–6565.
[37] M. Abe, *Vehicle Handling Dynamics: Theory and Application*. Oxford, U.K.: Butterworth-Heinemann, 2009.
[38] R. Ferber, I. M. Davis, D. S. W. Iii, and C. Laughton, "A comparison of within-and between-day reliability of discrete 3D lower extremity variables in runners," *J. Orthopaedic Res.*, vol. 20, no. 6, pp. 1139–1145, 2002.
[39] M. Spong, S. Hutchinson, and M. Vidyasagar, *Robot Modeling and Control*, vol. 3. New York, NY, USA: Wiley, 2006.
[40] J. Kong, M. Pfeiffer, G. Schildbach, and F. Borrelli, "Kinematic and dynamic vehicle models for autonomous driving control design," in *Proc. IEEE Intell. Vehicles Symp. (IV)*, Jun./Jul. 2015, pp. 1094–1099.
[41] J. Yi, J. Li, J. Lu, and Z. Liu, "On the stability and agility of aggressive vehicle maneuvers: A pendulum-turn maneuver example," *IEEE Trans. Control Syst. Technol.*, vol. 20, no. 3, pp. 663–676, May 2012.
[42] J. L. Campbell *et al.*, "Human factors design guidance for level 2 and level 3 automated driving concepts," Nat. Highway Traffic Safety Admin., Washington, DC, USA, Tech. Rep. DOT HS 812 555, 2018.
[43] C. C. Macadam, "Understanding and modeling the human driver," *Vehicle Syst. Dyn.*, vol. 40, nos. 1–3, pp. 101–134, 2003.
[44] S. H. Scott, "Optimal feedback control and the neural basis of volitional motor control," *Nature Rev. Neurosci.*, vol. 5, no. 7, pp. 532–546, 2004.
[45] S. H. Scott, "A functional taxonomy of bottom-up sensory feedback processing for motor actions," *Trends Neurosci.*, vol. 39, no. 8, pp. 512–526, 2016.
[46] H. Y. Choi *et al.*, "Experimental and numerical studies of muscular activations of bracing occupant," in *Proc. 19th ESV Conf., Paper*, 2005, pp. 1–10.
[47] S. Ejima, Y. Zama, K. Ono, K. Kaneoka, I. Shiina, and H. Asada, "Prediction of pre-impact occupant kinematic behavior based on the muscle activity during frontal collision," in *Proc. 21st ESV Conf.* 2009. pp. 909–913.
[48] J. He, W. S. Levine, and G. E. Loeb, "Feedback gains for correcting small perturbations to standing posture," *IEEE Trans. Autom. Control*, vol. 36, no. 3, pp. 322–332, Mar. 1991.
[49] N. Ogihara and N. Yamazaki, "Generation of human bipedal locomotion by a bio-mimetic neuro-musculo-skeletal model," *Biological*, vol. 84, no. 1, pp. 1–11, 2001.

Hideyuki Kimpara (M'16) received the B.S. and M.S. degrees from Keio University, Japan, in 1998 and 2000, respectively, and the Dr.Eng. degree from Nagoya University, Japan, in 2015. In 2000, he joined Toyota Central R&D Labs., Inc., Japan. While researching injury and rib fracture biomechanics, he visited the Bioengineering Center, Wayne State University, Detroit, MI, USA, from 2002 to 2006. In 2016, he was moved to the Future Research Department, Toyota Motor North America R&D, Ann Arbor, MI, USA, and assigned to human motion research with the Worcester Polytechnic Institute, Worcester, MA, USA, until 2019. His current research interests include human motion generation and prediction, robotics, applied biomechanics, and integrated safety for automotive or future mobility.

Kenechukwu C. Mbanisi (S'13) received the B.Eng. degree in electrical and electronic engineering from Covenant University, Nigeria, in 2013, and the M.S. degree in robotics engineering from the Worcester Polytechnic Institute, MA, USA, in 2018, where he is currently pursuing the Ph.D. degree in robotics engineering.

His research interests include human motion modeling, planning and analysis, and human–robot and human–machine interaction.

Jie Fu (M'12) received the M.Sc. degree in electrical engineering and automation from the Beijing Institute of Technology, Beijing, China, in 2009, and the Ph.D. degree in mechanical engineering from the University of Delaware, Newark, DE, USA, in 2013. Since 2016, she has been an Assistant Professor in robotic engineering with the Department of Electrical and Computer Engineering, Worcester Polytechnic Institute, Worcester, MA, USA. Her research interests include control theory, formal methods, machine learning, with applications to control design and verification of cyber-physical systems.

Zhi Li (M'10) received the M.S. degree in mechanical engineering from the University of Victoria, Victoria, BC, Canada, in 2009, and the Ph.D. degree in computer engineering from the University of California at Santa Cruz, CA, USA, Santa Cruz, in 2014. She was a Post-Doctoral Associate with Duke University from 2015 to 2016. She works on human–robot interaction, with application in telenursing robots, exoskeletons for stroke rehabilitation, and multi-arm surgical robots. She is currently an Assistant Professor with the Robotics Engineering Program, and the Mechanical Engineering Department, Worcester Polytechnic Institute, MA, USA. Her research focuses on computational human modeling, shared-autonomous robot motion coordination, and user-adaptive teleoperation interface.

Danil Prokhorov (SM'02) received the M.S. degree (Hons.) in Saint Petersburg, Russia, in 1992, and the Ph.D. degree in 1997. He joined the Staff of the Ford Scientific Research Laboratory, MI, USA. While at Ford, he pursued machine learning research focusing on neural networks with applications to system modeling, powertrain control, diagnostics, and optimization. He has been involved in research and planning for various intelligent technologies, such as highly automated vehicles, AI and other futuristic systems at the Toyota Tech Center, Ann Arbor, MI, USA, since 2005. Since 2011, he has been the Head of the Future Research Department, Toyota Motor North America R&D. He started his research career in Russia. He studied system engineering which included courses in math, physics, mechatronics, computer technologies, and aerospace and robotics. He has been serving as a Panel Expert for NSF, DOE, ARPA, as a Senior and Associate Editor for several scientific journals for more than 20 years. He has been involved with several professional societies, including the IEEE Intelligent Transportation Systems and the IEEE Computational Intelligence, and the International Neural Network Society (INNS) as its former Board Member, the INNS President, and was recently elected as an INNS Fellow. He has authored lots of publications and patents. Having shown feasibility of autonomous driving and personal flying mobility, his department continues research of complex multi-disciplinary problems while exploring opportunities for the next big thing.

Michael A. Gennert (SM'11) received the S.B. degree in CS, the S.B. degree in EE, the S.M. degree in EECS in 1980, and the Sc.D. degree in EECS in 1987 from MIT. He was with the University of Massachusetts Medical Center, the University of California at Riverside, Riverside, PAR Technology Corporation, and General Electric. He is currently a Professor of robotics engineering, CS, and ECE with the Worcester Polytechnic Institute, where he directs the WPI Humanoid Robotics Laboratory and was the Founding Director of the Robotics Engineering Program. He led WPI teams in the DARPA Robotics Challenge and the NASA Space Robotics Challenge. He has authored or co-authored more than 100 papers. His research has been supported by DARPA, NASA, NIH, NSF, and industry. His research interests include robotics, computer vision, and image processing, with ongoing projects in humanoid robotics, robot navigation and guidance, biomedical image processing, and stereo and motion vision. He is a member of Sigma Xi and a Senior Member of ACM.